

Pulse-Coupled Oscillator Networks: Do Small Worlds Synchronize Quicker?

Steven Hill

Complexity Science Doctoral Training Centre, University of Warwick, UK

June 28, 2008

Abstract

We numerically study the effects of topology on the synchronization time of directed pulse-coupled oscillator networks. Using an adapted version of the Watts-Strogatz small-world model, we initially show that small-world networks synchronize quicker than regular networks when the in-degree is fixed. In particular, we see a monotonically decreasing dependence of the synchronization time on the rewiring probability, which can be intuitively explained by the corresponding decrease in characteristic path length. Motivated by this, we instead fix the average characteristic path length. Our main result is that, in this case, small-world networks synchronize slower than regular networks and a non-monotonic dependence on the rewiring probability is observed. We also produce analytical results by studying the linearized dynamics and show that they are in good agreement with our numerical results.

1 Introduction

Motivated by empirical studies on the Internet, social and biological networks, the study of complex networks has become of considerable importance for the understanding of complex systems [1, 2]. Many studies are concerned with the structure of these networks and their evolution over time [3, 4]. Also of increasing interest is the collective behaviour of interacting dynamical systems on networks and the effect of the network structure on the dynamics [1, 5, 6].

One of the simplest and most studied types of collective dynamics on networks is synchronization (for an overview see [7, 8]). Many real-world systems, both artificial and natural, are known to exhibit this phenomenon. Examples include Josephson junction arrays [9], fireflies flashing [10] and neural networks [11]. Neural networks are the basis of the model discussed in this paper.

Neurons in the brain communicate by sending and receiving brief electrical pulses called spikes or action potentials [12]. A spike causes a change in the membrane potential of the recipient neuron. Hence we consider pulse-coupled networks in which the interactions take place at discrete instances in time only. These have already received much interest [13, 14, 15, 16] due to their applicability to many natural systems. Unlike many of these studies, our model incorporates a delay between a neuron firing (sending a spike) and a connected neuron receiving the spike. This arises due to the spikes finite propagation speed. We also consider directed networks as a pair of neurons don't necessarily communicate in both directions.

It is important to study synchronization on neural networks since it is known to be involved in information transmission, pattern recognition and learning. However, it could also be a factor in diseases such as epilepsy and Parkinson disease [17].

The topology of networks is known to influence synchronization, but many studies consider only either regular or random coupling only [18, 19, 20]. One area that has been investigated with varying topology is the synchronizability of networks [6, 21]. This is a measure of how easily a network can be synchronized in terms of the coupling parameters. It is shown in [6] that small-world networks (regular locally clustered networks with the addition of a few long-range edges [5]) are more synchronizable than regular networks. Topology is particularly important for synchronization on neural networks as here the connectivity is very complex [22] and the networks may even have small-world properties (for example, the *C.elegans* neural network [23]).

In this paper we numerically study the effect of topology on the synchronization time of pulse-coupled directed neural networks. Synchronization time is a measure of how quickly the network re-synchronizes after being perturbed from a synchronized state. It has been studied analytically for fully random networks only [20]. We produce networks of different topologies using an adapted version of the Watts-Strogatz small-world model [5]. Firstly, it is shown that for networks with a fixed number of edges,

those in the small-world regime synchronize quicker than regular networks. This is expected due to the result for synchronizability mentioned above and the dependence can be intuitively explained by the shorter average characteristic path length between nodes in a small-world network. However, other factors are important for synchronization other than the characteristic path length [24]. Hence, we fix the average characteristic path length and again investigate the dependence of synchronization time on topology. We find that, for a fixed average characteristic path length, networks in the small-world regime synchronize slower than regular networks. In particular, we see a non-monotonic dependence on the rewiring probability. Finally, we make a comparison with analytical results.

The paper is organised as follows. Section 2 outlines the neural dynamics, basic network topology definitions and introduces the directed small-world network model. The synchronized state is also explained here. In Section 3 we identify when the small-world networks occur and give the result for the dependence of synchronization time on topology for networks with a fixed number of edges. Section 4 explains the method for fixing the average characteristic path length and the simulation and analytical methods are outlined. Synchronization time is defined here also. In Section 5 we give the results and discuss them. A comparison is made between the simulated and analytical results. We close in Section 6 with a summary and a discussion of further work.

2 Model and Definitions

2.1 Neuron dynamics model

We consider a pulse-coupled directed network of N neural oscillators with delayed interactions. The model described below is based on that of Mirollo and Strogatz [13] and was also used by Timme *et al.* [20].

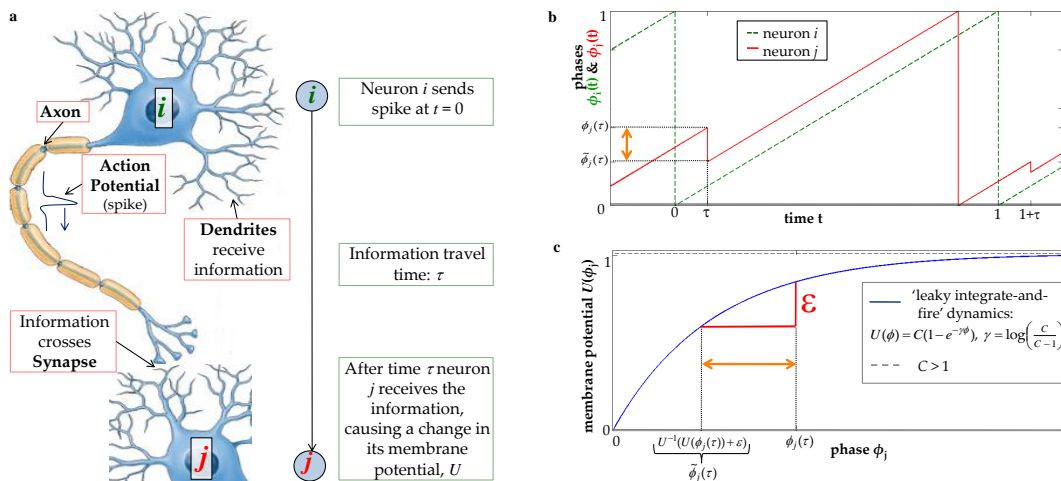


Figure 1: Neuron Dynamics. (a) A schematic depicting how neurons communicate. (b) Neuron i spikes at time $t = 0$ and neuron j receives this spike at time $t = \tau$, causing a decrease in its phase. (c) The membrane potential function determines the size of the phase decrease.

The simple schematic example in Figure 1 explains how the neurons behave and interact. Figure 1(a) shows a neuron i in communication with a neuron j . It is assumed neuron i has no incoming spikes (i.e. no pre-synaptic oscillators) and neuron j receives spikes from neuron i only.

The state of a neuron i at time t is given by a phase-like variable $\phi_i(t) \in (-\infty, 1]$. In the absence of interactions this phase increases linearly with time, $\frac{d\phi_i}{dt} = 1$.

When a threshold is reached, $\phi_i(\hat{t}_f) = 1$, the phase is instantaneously reset to zero (see Figure 1(b), where we have taken $\hat{t}_f = 0$). At this moment the neuron fires and sends a spike along its axon and across the synapse to connected (post-synaptic) neurons. These post-synaptic neurons receive the incoming signal after a time delay τ (i.e. at $\hat{t}_f + \tau$). The effect of this interaction is an instantaneous change of size ϵ in the membrane potential $U(\phi)$ of the post-synaptic neurons. As in [20] we consider only inhibitory coupling ($\epsilon < 0$) and we also take it to be homogeneous across all couplings. A decrease in membrane potential by an amount ϵ causes the phase of a post-synaptic oscillator to instantaneously jump from $\phi(\hat{t} + \tau)$ to $U^{-1}(U(\phi(\hat{t} + \tau)) + \epsilon)$ as seen in Figure 1(c).

The function U is assumed to be monotonically increasing ($U' > 0$), concave down ($U'' < 0$) and satisfies $U(0) = 0$, $U(1) = 1$. In this work we use the well-known leaky integrate-and-fire type dynamics [13] given by

$$U(\phi) = C(1 - e^{-\gamma\phi}) \quad \text{where } \gamma = \log\left(\frac{C}{C-1}\right), \quad C > 1. \quad (1)$$

We choose this function as it greatly simplifies the analytics of the linearised dynamics, which we use to produce our analytical results (see Section 4.3).

2.2 Network topology

We study networks with varying topology. Firstly, we give some basic definitions. Recall that N is the number of nodes (neurons) in the network (in all our simulations we used $N = 1000$).

We define L to be the *characteristic path length* of a network. This is the number of edges in the shortest directed path between two distinct nodes, averaged over all $N(N-1)$ ordered node pairs. Note that this implies that we must only consider strongly connected networks (that is, networks in which a directed path exists between all pairs of nodes).

Another important quantity is the *clustering coefficient*, C . The clustering coefficient of an individual node i is found by counting the number of actual triplets containing node i and then dividing this number by the number of possible triplets containing node i (see Figure 2). The clustering coefficient is the result after averaging over all nodes. It is a measure of the local structure in the network.

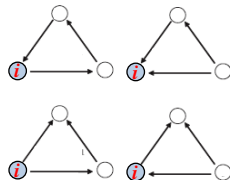


Figure 2: Actual triplets containing node i . The two white nodes are arbitrary and so can be interchanged along with their attached edges. For example, in the top left triplet all the edges can be reversed and this is equivalent to the triplet already displayed (to see this imagine picking up the top white node and moving it below the other two whilst keeping the edges attached).

The above two definitions are based on those in [5] but adapted for directed networks. The clustering coefficient definition is taken from [26]; a full explanation of how to calculate it can be found there.

A final definition is for the *average in-degree* of a network, k . This is the number of edges entering an individual node, averaged over all nodes. This is a standard definition in graph theory [27].

To produce networks of varying topology we use a model based on that of Watts and Strogatz [5] but adapted for directed networks. We start with a ring of N nodes, each of which is connected to its k nearest neighbours via k directed edges (k is chosen to be even). Hence we have Nk edges in the network and every node has the same in-degree of k . This obviously means the average in-degree of the network is also k . With probability p , the tail/base of each edge is rewired to another node chosen uniformly at random from the whole network, but duplicate edges and edges from a node to itself are not allowed. We do however allow the edge to be ‘rewired’ back to its original position.

An important observation here is that as p varies the in-degree of each node (and the average in-degree of the network) is still k . This is due to the fact we only rewire tails. So in what follows we only refer to this single quantity k .

As the rewiring probability p is changed from 0 to 1 the network interpolates between regular and random topologies (see Figure 3). In Section 3.1 we show that for small values of p we see small-world networks as in the original Watts-Strogatz model. These networks are characterised by a large clustering coefficient and small characteristic path length.

2.3 The synchronized state

There are many different levels and types of synchronization on a network. For example only part of the network may be synchronized, the network may synchronize in distinct clusters [14] or the neurons may fire in a periodic firing pattern [28]. In this work we study global synchronization, which is the strongest and possibly simplest form of synchronization on pulse-coupled oscillator networks (see Figure

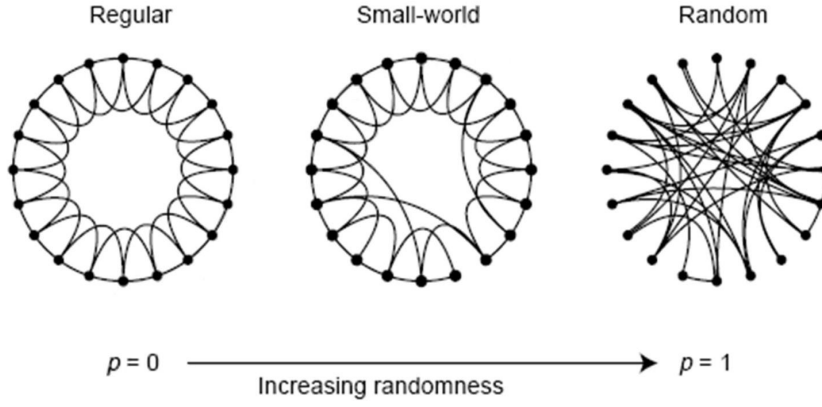


Figure 3: The transition from regular to random networks for the original Watts-Strogatz model. p is the rewiring probability. Our model is similar but for every edge displayed here, we have two edges; one in each direction. We only rewire the tails of these directed edges.

4(a)). This is when all the neurons have identical phases and hence all fire at the same time, i.e.

$$\phi_i(t) = \phi_j(t) \quad \forall i, j \in \{1, 2, \dots, N\}, \quad \forall t \in \mathbb{R} \quad (2)$$

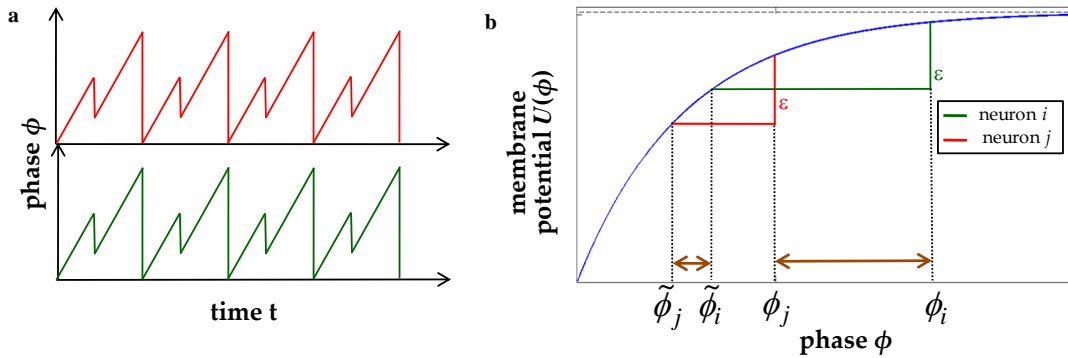


Figure 4: (a) The globally synchronized state. (b) An intuitive explanation for asymptotic stability of the globally synchronized state. Two neurons receiving spikes at the same moment experience a contraction of their phases: $|\tilde{\phi}_j - \tilde{\phi}_i| < |\phi_j - \phi_i|$.

In order for the globally synchronized state to exist, all the neurons need to receive spikes at the same time and the total effect of these spikes on the membrane potential has to be the same for all neurons. This latter property is referred to as normalized coupling in the literature [20] and in general is given by the constraint

$$\sum_j \epsilon_{ij} = \alpha \quad \text{for all } i \quad (3)$$

where ϵ_{ij} is the coupling strength of spikes sent from neuron j to neuron i (if there is no edge from neuron j to i then $\epsilon_{ij} = 0$) and α is a constant. Hence the sum gives the total coupling strength for all spikes received by neuron j each period. Our model satisfies these properties since we consider a homogeneous delay time τ and coupling strength $\epsilon_{ij} = \epsilon$ across all connected neuron pairs and the in-degree of each node is always k . So after a time τ from all the neurons firing, they all receive k spikes causing the membrane potential of each neuron to decrease by $\alpha = k\epsilon$.

An important question is whether this globally synchronized state is stable to small perturbations and moreover, if it is asymptotically stable. Indeed, we are interested in synchronization time which is a measure of how quickly the network re-synchronizes after being perturbed away from this state. Hence we need asymptotic stability for this to make sense. It has been proven by Timme and Wolf [25] that, for inhibitory normalised coupling, this state is indeed asymptotically stable under the mild condition

of the network being strongly connected. As mentioned above, we already only consider networks with this property. An intuitive explanation for this asymptotic stability can be seen in Figure 4(b). Due to the concavity of the membrane potential function U , two neurons receiving a spike at the same time experience a contraction of their phases.

A final question relating to the synchronized state is how small the perturbations have to be for re-synchronization to occur. We deal with this question in Section 4.2.

3 Preparatory results

3.1 Identification of the small-world regime

We see that for our adapted Watts-Strogatz model, the dependence of the normalised average clustering coefficient $\frac{\langle C(p) \rangle}{C(0)}$ and normalised average characteristic path length $\frac{\langle L(p) \rangle}{L(0)}$ on the rewiring probability p is the same as that seen in the original model [5]. Here, the averages are over realizations of networks. Figure 5 shows the numerical results for a couple of k values. Note that we always plot p on a logarithmic scale to resolve the fast drop in $\langle L(p) \rangle$. It is this fast drop that gives a range of p values where, on average, the networks have small characteristic path lengths (i.e. near the value for a fully random network) but the clustering coefficient is still high (i.e. almost the same as its value for a fully regular network). Networks with this property are known as small-world.

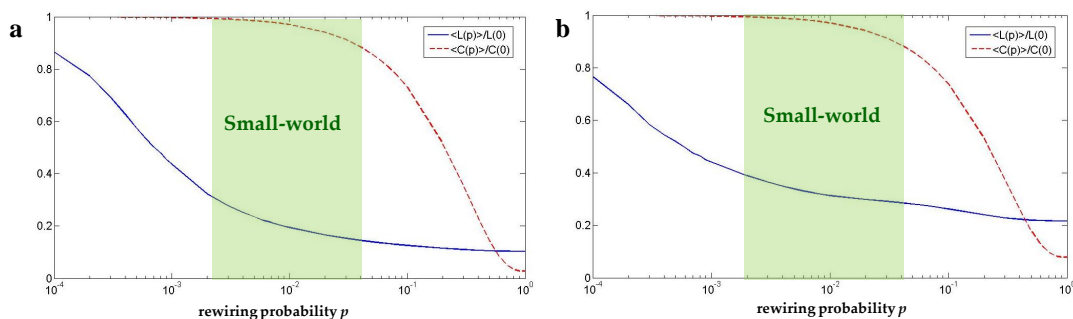


Figure 5: Normalised average characteristic path length $\frac{\langle L(p) \rangle}{L(0)}$ and normalised clustering coefficient $\frac{\langle C(p) \rangle}{C(0)}$ against rewiring probability p for networks with in-degree k fixed at: (a) $k = 20$, (b) $k = 58$. ($N = 1000$. Plots produced with 38 values of p . Averages are over 100 realizations of networks produced by the rewiring process described in Section 2.2).

The fast decrease in the characteristic path length of a network is a result of the creation of a few long-range edges in the rewiring process. However, the local structure remains largely unchanged and so there is little effect on the clustering coefficient. We see that the small-world region (which isn't rigorously defined) varies with k , but only in a minor way. It is worth noting that work has been done on identifying when the crossover from regular to small-world occurs [29] but the focus has been on the system size N rather than the nodal degree k .

3.2 Synchronization time for networks of fixed in-degree

In this Section we present the numerical results for the dependence of average synchronization time $\langle \tau_{sync}(p) \rangle$ on the rewiring probability p for networks of fixed in-degree k . The simulation method and definition of synchronization time are in Section 4.2. For now, recall that synchronization time is a measure of how quickly a network re-synchronizes after being perturbed from a globally synchronized state. We present this result here as it motivates studying the average synchronization time of networks with fixed average characteristic path length $\langle L(p) \rangle$.

The result is displayed in Figure 6 for one value of k . The averages are over realizations of networks and perturbations. We see that $\langle \tau_{sync}(p) \rangle$ is monotonically decreasing with p . In particular, small-world networks re-synchronize quicker than regular networks and random networks re-synchronize the quickest. This dependence can be explained by the average characteristic path length. Indeed, the dependence of $\langle L(p) \rangle$ on p is also monotonically decreasing in a similar fashion (see Figure 5(a)). It is intuitive that as the characteristic path length decreases, neurons on one side of the network can communicate more efficiently with neurons on the opposite side and this leads to quicker and more efficient re-synchronization.

We now fix the average characteristic path length $\langle L(p) \rangle$ as it is known this is not the only topological factor in synchronization [24] but appears to be the dominating one in the synchronization time result for

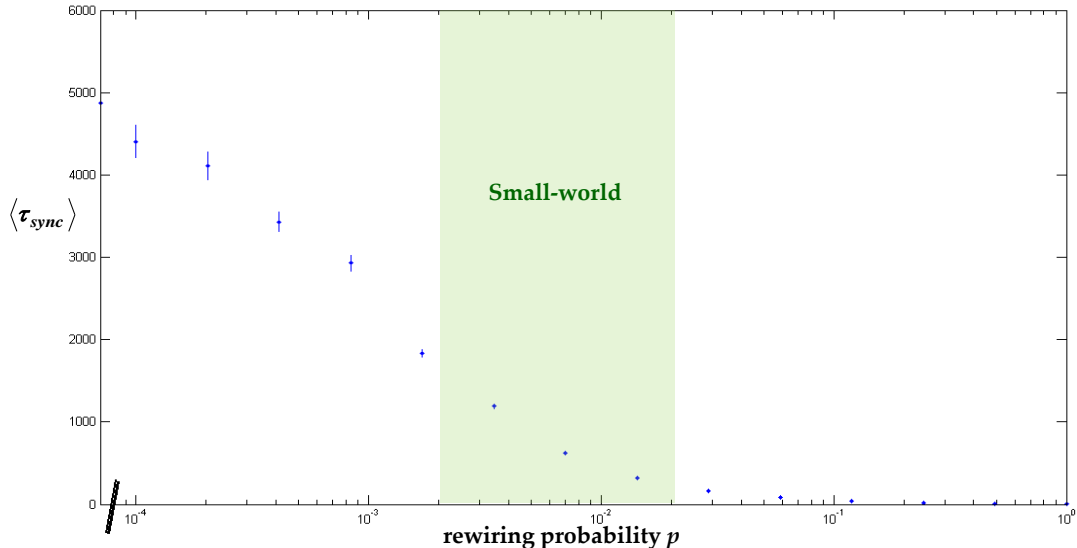


Figure 6: Average synchronization time $\langle \tau_{sync}(p) \rangle$ against rewiring probability p for networks with in-degree fixed at $k = 20$. Error bars are standard errors of the mean. (Parameters used: $N = 1000$, $k = 20$, $C = 1.01$, $\alpha = k\epsilon = -0.2$, $\tau = 0.1$, $\delta = 0.01$).

fixed in-degree k . Fixing this quantity (and varying k instead) allows us to investigate how synchronization time depends on the rewiring probability for a different ensemble of networks. In particular, we see if small-world networks still re-synchronize quicker than regular ones in this case and it gives us some insight into how topological factors other than the characteristic path length influence synchronization time.

4 Method

4.1 Method for fixing average characteristic path length

We fix the average characteristic path length $\langle L(p) \rangle$ using a graphical method. Figure 7 shows how $\langle L(p) \rangle$ depends on the rewiring probability p for many different values of k . Note that, unlike in Figure 5, the values here are unnormalized. We choose to fix $\langle L(p) \rangle = 4$ (see Figure 7 inset) as this gives us a wide range of p values. We do not take $k < 6$ as the networks are in general no longer strongly connected for larger p values. Any realizations that produce networks that are not strongly connected are discarded and repeated (this happened in the $k = 6$ case only). For each of these in-degree values a value of the rewiring probability p is found from the plot that gives $\langle L(p) \rangle \approx 4$. The value of k which gives a characteristic path length for the fully regular graph nearest $L(0) = 4$ was also found (the result being $k = 142$). This gives us 25 (k, p) pairs to use in the simulations.

We note that k decreases in a non-linear fashion as p increases for networks with $\langle L(p) \rangle = 4$. When we increase p , we decrease the in-degree k . Thus, it might be expected that the amount of coupling each neuron receives also decreases (recall that the total change in membrane potential each period due to incoming spikes is $\alpha = k\epsilon$). This would affect the synchronization time [30]. We remove this factor by keeping $k\epsilon$ fixed as p varies. By doing this, we have reduced the effect of changing the in-degree k on the synchronization time.

The result of using this method to fix $\langle L(p) \rangle$ can be seen in Figure 8. We see that for each (k, p) pair we get $\langle L(p) \rangle \approx 4$ as required. Note that the standard deviations are larger for smaller p values. This is because we are rewiring a small number of edges here (Nk/p on average); the effect on $L(p)$ of rewiring $m + 1$ edges instead of m edges where m is small can be large as it may add a long-range edge where there was not one previously.

4.2 Simulation method and Synchronization time definition

We now describe the initial condition used for the simulations and how the synchronization time was measured.

The initial condition for the phases of the neurons is a random perturbation from the globally synchronized state (2) and in particular is applied to $\phi_i = 0$ for all i . The perturbation is given by a vector

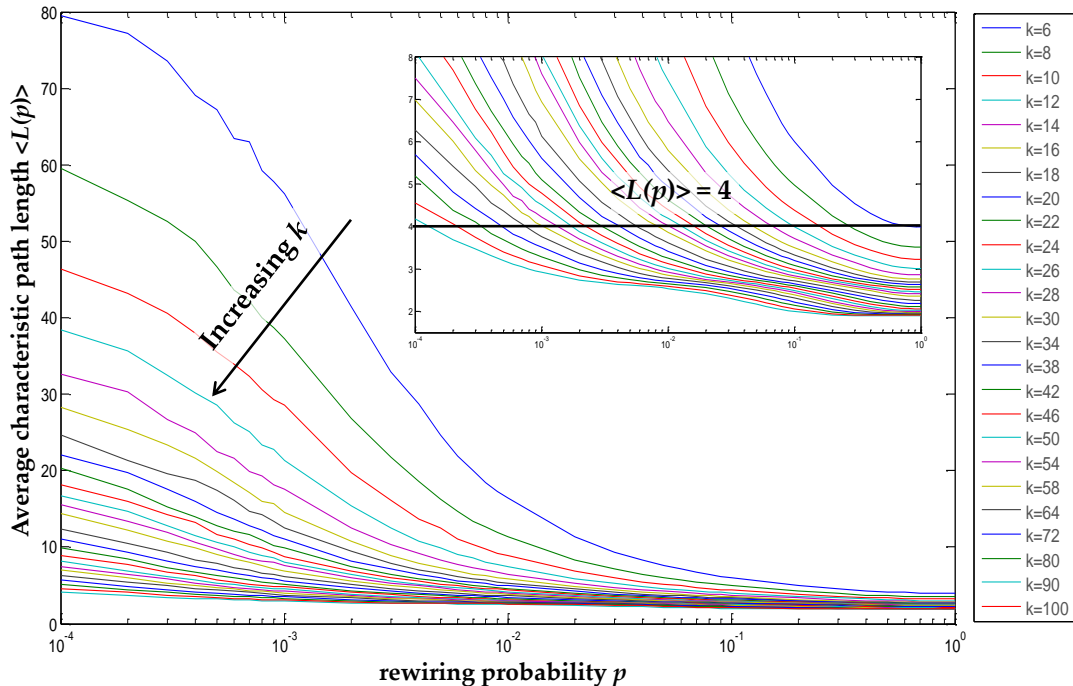


Figure 7: Average characteristic path length $\langle L(p) \rangle$ against rewiring probability p for 24 values of in-degree k . We fix $\langle L(p) \rangle = 4$ using this plot by finding the (k, p) pairs that give this value. ($N = 1000$. Each line produced with 38 values of p . Averages are over 100 realizations of networks).

$\mathbf{d}^0 \in \mathbb{R}^N$ where the components d_i^0 are each drawn independently from a uniform distribution on $[-\delta, \delta]$. d_i^0 is the perturbation applied to neuron i . So the initial condition for neuron i is

$$\phi_i(0) = 0 + d_i^0. \quad (4)$$

To ensure that the globally synchronized state is stable we have the condition $\delta < \frac{\tau}{2}$ [20] (recall that τ is the delay time). This guarantees that all the neurons fire before any spikes are received. We note that the perturbation can make the starting phase of a neuron negative. When this phase increases to zero, the neuron does not fire. This is also the case when a spike causes a phase to become negative.

As we want to know how quickly the neurons re-synchronize, we need a measure of how close the network is to the globally synchronized state at time t . We define a distance vector $\mathbf{d}(t) \in \mathbb{R}^N$ where the components $d_i(t) \in (-0.5, 0.5]$ give the distance of neuron i from the globally synchronized state at time t . In the simulations a reference oscillator r is chosen (since the networks and perturbations are random the same neuron can be chosen in each realization). This reference neuron fires at discrete times, which we denote by \hat{t}_j where $j \in \mathbb{N}$ and $\hat{t}_j < \hat{t}_{j+1}$. At these instances (i.e. when $\phi_r(\hat{t}_j) = 0$) we measure the distance from the globally synchronised state ($\phi_i(\hat{t}_j) = 0$ for all i). The distance is given by the infinity norm of $\mathbf{d}(t)$, $\|\mathbf{d}(t)\|_{\max}$. So at times \hat{t}_j we have,

$$\|\mathbf{d}(\hat{t}_j)\|_{\max} = \max_i |d_i(\hat{t}_j)| \quad \text{where} \quad d_i(\hat{t}_j) = \begin{cases} \phi_i(\hat{t}_j) & \text{if } \phi_i(\hat{t}_j) \leq 0.5 \\ \phi_i(\hat{t}_j) - 1 & \text{if } \phi_i(\hat{t}_j) > 0.5 \end{cases} \quad (5)$$

Note that here we have $\mathbf{d}(0) = \mathbf{d}^0$ using this definition.

For each (k, p) pair 100 realizations were carried out in order to average over networks and perturbations. Figure 9 shows the distance from the synchronized state (on a logarithmic scale) against time for all the realizations from one (k, p) pair. We see some transient behaviour before the distance decays exponentially (or to be more precise, approaches exponential decay, see Section 5). The synchronization time τ_{sync} is defined in terms of the exponential exponent of this decay,

$$\|\mathbf{d}(t)\|_{\max} = \exp\left(-\frac{t}{\tau_{sync}}\right). \quad (6)$$

We find the synchronization time for each realization by using least squares linear regression to find the gradient of the line between two time points. These time points are chosen as high as possible since exponential decay is approached as $t \rightarrow \infty$, but far enough apart so that there is sufficient data

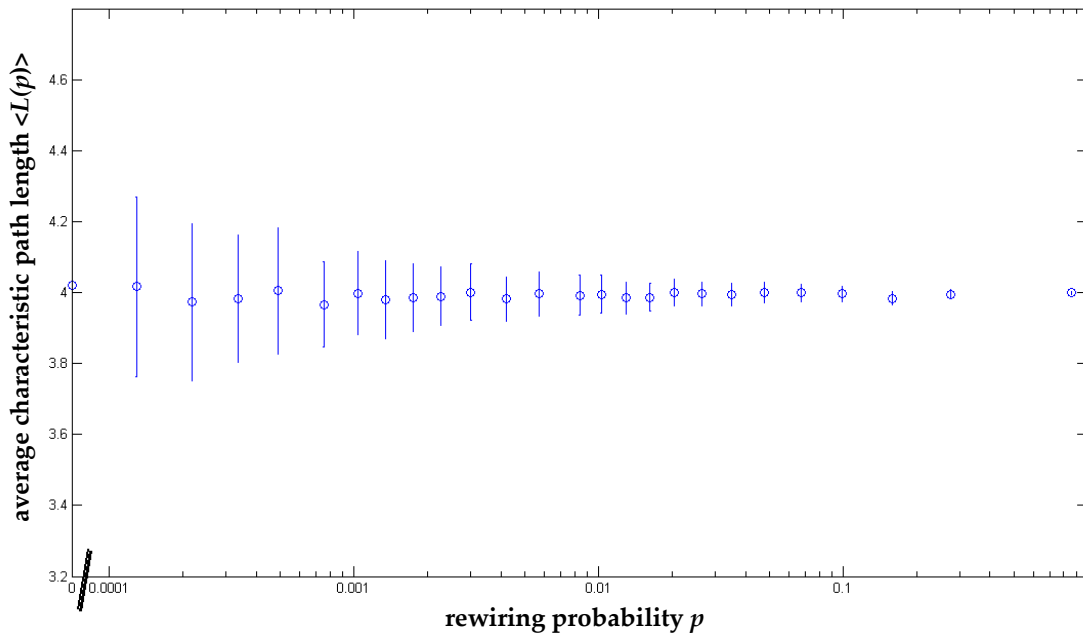


Figure 8: Average characteristic path length $\langle L(p) \rangle$ against rewiring probability p for each (k, p) pair used in the simulation. Error bars are standard deviations. ($N = 1000$. Averages are over 100 realizations of networks).

to perform the regression accurately. We also want to avoid very small distances, which introduce significant numerical error in the simulation. Finally, we average over all realizations to give the average synchronization time $\langle \tau_{sync} \rangle$.

4.3 Analytical method

We adapt the work by Timme *et al.* to produce some analytical results for comparison with our numerical results. Full details of this work can be found in [20] and [25].

In our numerical method we defined a distance vector $\mathbf{d}(t)$ which gives the distance of each neuron from the globally synchronized state. Let T be the period of this state. Explicitly we have $T = \tau + 1 - U^{-1}(U(\tau) + k\epsilon)$. We still assume the perturbation is applied as in (4) at time $t = 0$.

In order to analytically find the synchronization time we define a stroboscopic period- T map, $F : \mathbb{R}^N \rightarrow \mathbb{R}^N$. (Note that in the numerical method, we sampled $\mathbf{d}(t)$ at irregular time intervals). The map F is given by $F(\mathbf{d}_j) = \mathbf{d}_{j+1}$ for $j = 0, 1, 2, \dots$ where $\mathbf{d}_j = \mathbf{d}(jT + 1)$ and $\mathbf{d}(jT + 1)$ is given by (5) (replacing \hat{t}_j with $jT + 1$). Here we have $\mathbf{d}_0 = \mathbf{d}(1) = \mathbf{d}(0)$ since no spikes are received before all the oscillators reach the phase threshold for the first time. Hence we first apply the map F in the first period when spikes are received.

We want to linearize the map F . This map depends on the network connectivity, membrane potential function U and the dynamical parameters τ and ϵ_{ij} . The linearized map is given by a matrix $A \in \mathbb{R}^{N \times N}$ which results in a first order map $\mathbf{d}_{j+1} = A\mathbf{d}_j$ for $j = 0, 1, 2, \dots$. It has been shown [25] that for general membrane potential functions and normalized coupling (3), the matrix A not only depends on the properties mentioned above, but also on the vector \mathbf{d}_j . In particular, it depends on the order of the components of \mathbf{d}_j after they are put into ascending order. Hence we have a multi-operator problem. However, we use integrate-and-fire dynamics (1) which are shown in [20] to be a degenerate case where the matrix A is now independent of the rank order of \mathbf{d}_j .

It turns out that the linearized map A is given by a sparse matrix

$$A_{ij} = \begin{cases} \frac{-\epsilon}{Ce^{-\gamma\tau} - \alpha} & \text{if there exists an edge from neuron } j \text{ to neuron } i \\ 1 + \frac{\alpha}{Ce^{-\gamma\tau} - \alpha} & \text{if } i = j \\ 0 & \text{otherwise} \end{cases} \quad (7)$$

where $\alpha = k\epsilon$ is the total coupling strength. Since each neuron has in-degree k the row-sums of the matrix A are all equal to one.

We let \mathbf{v}_i for $i = 1, 2, \dots, N$ be the eigenvectors of A with corresponding eigenvalues $|\lambda_1| > |\lambda_2| > \dots > |\lambda_N|$. The largest eigenvalue $|\lambda_1| = 1$ and is unique (this can be shown using the Gershgorin circle

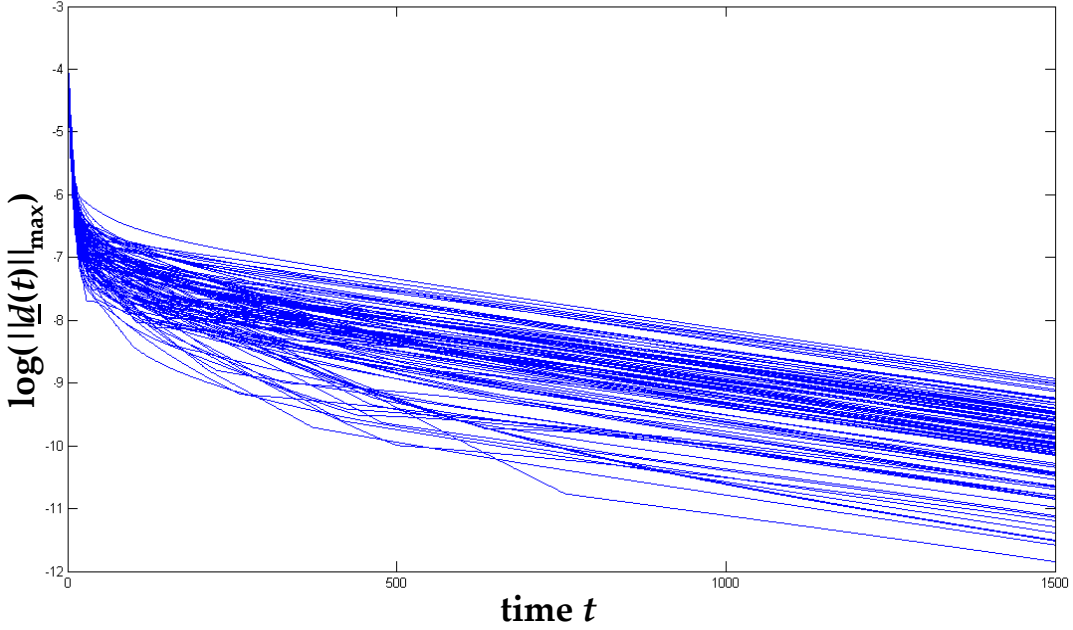


Figure 9: Logged distance from the globally synchronized state against time for the 100 realizations from one (k, p) pair. Both network and perturbation are random for all realizations. (Parameters used: $N = 1000$, $k = 58$, $\langle L \rangle = 4$, $C = 1.01$, $\alpha = k\epsilon = -0.2$, $\tau = 0.1$, $\delta = 0.01$).

theorem and Perron-Frobenius theorem [31]). The corresponding eigenvector is $\mathbf{v}_1 = (1, 1, \dots, 1)^\top$ since the row-sums of A are equal to one. We note that this means the distance vector \mathbf{d}_j does not tend to zero as $j \rightarrow \infty$ as they did in the numerical method. Instead, it tends to a uniform phase shift \mathbf{d}_∞ which has all components equal, $(\mathbf{d}_\infty)_i = d_\infty$ for all i (i.e. all the neurons are the same distance from threshold and hence in a globally synchronized state). To illustrate this we take a simple example. If the neurons are initially all perturbed by the same amount, $\phi_i(0) = \tilde{\delta}$ for all i , then they start off globally synchronized and $\mathbf{d}(0) = \mathbf{d}_j = (\tilde{\delta}, \tilde{\delta}, \dots, \tilde{\delta})^\top$ for all j .

So the distance from the globally synchronized state is now given by $\|\mathbf{d}(t) - \mathbf{d}_\infty\|_{\max} = \|\mathbf{d}(t)\|_{\max} - d_\infty$. Using the fact that $\lambda_1 = 1$, $\mathbf{v}_1 = (1, 1, \dots, 1)^\top$ and rewriting \mathbf{d}_0 as a linear combination of the basis of eigenvectors gives

$$\mathbf{d}_j - \mathbf{d}_\infty = A^j \mathbf{d}_0 - \mathbf{d}_\infty = A^j \left(\sum_{i=1}^N \beta_i \mathbf{v}_i \right) - d_\infty \mathbf{v}_1 = (\beta_1 - d_\infty) \mathbf{v}_1 + \sum_{i=2}^N \beta_i \lambda_i^j \mathbf{v}_i. \quad (8)$$

Since $(\mathbf{d}_j - \mathbf{d}_\infty) \rightarrow \mathbf{0}$ as $j \rightarrow \infty$ and $|\lambda_i| < 1$ for $i \geq 2$ it follows from (8) that

$$\lim_{j \rightarrow \infty} \left[(\beta_1 - d_\infty) \mathbf{v}_1 + \sum_{i=2}^N \beta_i \lambda_i^j \mathbf{v}_i \right] = (\beta_1 - d_\infty) \mathbf{v}_1 = \mathbf{0} \quad (9)$$

and hence

$$\beta_1 = d_\infty. \quad (10)$$

Then, since λ_2 is the second largest eigenvalue, taking the infinity norm in (8) gives

$$\|\mathbf{d}_j - \mathbf{d}_\infty\|_{\max} = \left\| \sum_{i=2}^N \beta_i \lambda_i^j \mathbf{v}_i \right\|_{\max} = \left| \beta_2 \lambda_2^j \right| \left\| \mathbf{v}_2 + \sum_{i=3}^N \frac{\beta_i}{\beta_2} \left(\frac{\lambda_i}{\lambda_2} \right)^j \mathbf{v}_i \right\|_{\max} \sim |\beta_2| |\lambda_2|^j \|\mathbf{v}_2\|_{\max} \quad (11)$$

where \sim means ‘is asymptotically equal to (as $j \rightarrow \infty$)’.

Taking the logarithm gives

$$\log(\|\mathbf{d}_j - \mathbf{d}_\infty\|_{\max}) \sim \omega + j \log |\lambda_2| \quad (12)$$

where ω is a constant.

We recall that \mathbf{d}_j is the distance vector at time $jT + 1$ and asymptotically define the analytical synchronization time by

$$\|\mathbf{d}_j - \mathbf{d}_\infty\|_{\max} \sim |\beta_2| \|\mathbf{v}_2\|_{\max} \exp\left(-\frac{jT + 1}{\tau_{sync}}\right) \quad (13)$$

which after taking the logarithm gives

$$\log(\|\mathbf{d}_j - \mathbf{d}_\infty\|_{\max}) \sim \omega - \frac{jT + 1}{\tau_{sync}}. \quad (14)$$

Comparing (12) with (14) we see that

$$\lim_{j \rightarrow \infty} \frac{\omega - \frac{jT+1}{\tau_{sync}}}{\omega + j \log|\lambda_2|} = 1 \quad (15)$$

from which it follows that

$$\tau_{sync} = -\frac{T}{\log|\lambda_2|}. \quad (16)$$

We numerically find the second largest eigenvalue of the matrix A and use this to calculate the analytical synchronization time (16). The average synchronization time $\langle \tau_{sync} \rangle$ is then obtained by averaging over realizations of networks.

5 Main result and Discussion

The result for the dependence of numerical and analytical average synchronization time $\langle \tau_{sync} \rangle$ on the rewiring probability p for network ensembles with fixed average characteristic path length $\langle L(p) \rangle$ is shown in Figure 10.

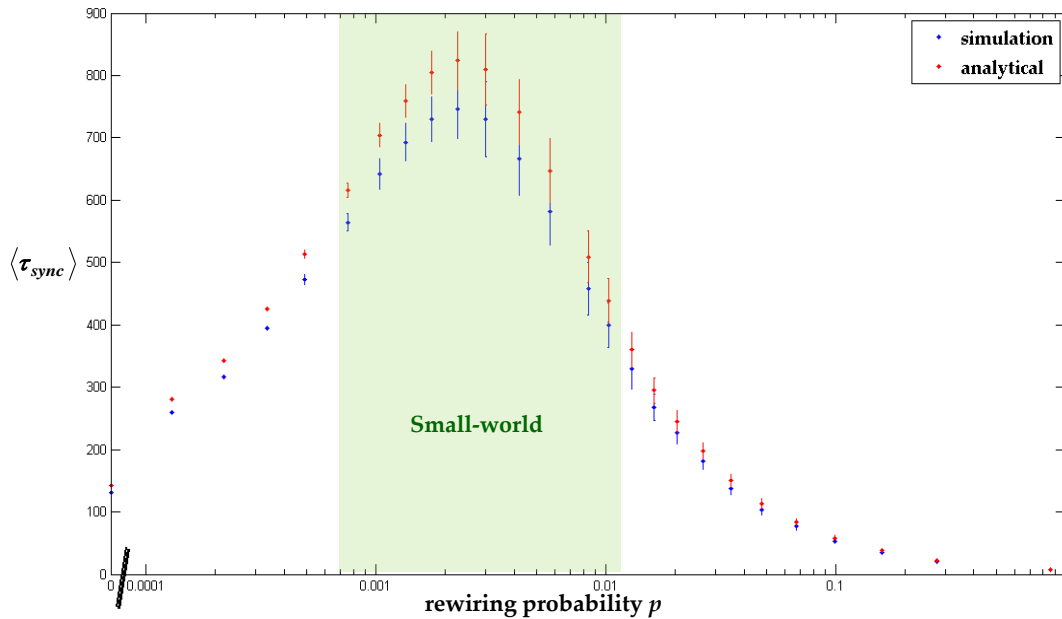


Figure 10: Average numerical and analytical synchronization time $\langle \tau_{sync} \rangle$ against rewiring probability p for networks with fixed average characteristic path length $\langle L(p) \rangle = 4$. Error bars are standard deviations. Small-world region is determined by taking each (k, p) pair and seeing if this puts it in the small-world region on plots as in Figure 5. Average synchronization time is averaged over 100 realizations, varying network and perturbation each time. (Parameters used: $N = 1000$, $\langle L \rangle = 4$, $C = 1.01$, $\alpha = k\epsilon = -0.2$, $\tau = 0.1$, $\delta = 0.01$).

We first discuss the numerical result. We see that in the small-world regime, the average synchronization times are the highest. This means that for network ensembles of fixed average characteristic path length, those with regular topology actually synchronize quicker than those with the small-world property. This contradicts the popular belief that small-world networks exhibit more efficient synchronization properties than regular networks [5, 6], which we have shown is true for networks of fixed in-degree k (see Section 3.2). We still see that random networks are the quickest at synchronizing.

The dependence of $\langle \tau_{sync} \rangle$ on p for the fixed k networks is monotonically decreasing and can be intuitively explained by the average characteristic path length which follows a similar dependence. The result here for fixed $\langle L(p) \rangle$ has a non-monotonic dependence on p . Hence, a possible reason for this behaviour is not as clear as with the fixed k result. The in-degree k is monotonically decreasing with p and it can be shown that the clustering coefficient $\langle C(p) \rangle$ is also monotonically decreasing. So neither of

these topological properties alone give an obvious explanation. One possibility is that it could be due to an interplay between more than one network property. For example, the fast synchronization of regular networks could be due to the in-degree k being large. This is not because the total coupling strength $\alpha = k\epsilon$ is high, as we kept this fixed for all (k, p) pairs (see Section 4.1), but could be because the neurons receive the coupling effect from a large number of spikes. However, we also see fast synchronization for random networks where k is small and so the same total coupling amount is received from far fewer spikes. The reason for fast synchronization here could simply be because the network is indeed random. So we can see that the explanation for the non-monotonic dependence is non-trivial. It may even be necessary to define a new network property to explain the relationship properly.

The analytical results match the numerical results well. We see the same non-monotonic behaviour and the standard deviations are also very similar. This implies that the linearized map used in the analytical method is a good approximation to the actual dynamics. We do see that the analytical values are systematically higher than the corresponding numerical values and the difference appears to be greater in the small-world region. This can be explained by the non-exponentiality of the decay of the distance from the globally synchronized state $\|\mathbf{d}(t)\|$ for finite times (the analytics show this, see equation (11)). In our numerical method we measure the gradient of the decay between two finite times t_1 and t_2 . We found that increasing t_1 or t_2 can give a shallower gradient and hence a larger average synchronization time $\langle\tau_{sync}\rangle$. This suggests that if the simulation was run for longer we may in some cases get higher numerical results as the decay is closer to being exponential.

6 Conclusion and Further Work

We have investigated the effect of topology on the synchronization time of pulse-coupled neural oscillator networks, looking in particular at regular, small-world and random networks.

Firstly, we saw that for networks of fixed in-degree k , the average synchronization time $\langle\tau_{sync}\rangle$ was monotonically decreasing with the rewiring probability p . This was explained by the corresponding decrease in the average characteristic path length $\langle L(p)\rangle$. So we have shown that in this case small-world networks synchronize quicker than regular networks.

Secondly, instead of fixing the in-degree, we fixed the average characteristic path length. We then saw that networks in the small-world regime synchronize slower than regular networks and a non-monotonic dependence on the rewiring probability was observed. This result is surprising given the common belief that small-world networks exhibit more effective synchronization than regular networks. An explanation for this dependence is yet to be found.

Finally, we compared our numerical synchronization time results to analytical results. These were calculated from the eigenvalues of the linearized dynamics. We saw that the analytical results gave the same non-monotonic dependence on the rewiring probability and were in good agreement with the numerics (only a small systematic difference was observed). This suggests that the linearized dynamics are a good approximation and may be useful in understanding the behaviour we have observed.

This work has many useful extensions. We have so far only obtained the results for one set of parameters. It would be useful to discover if we get the same results for different parameters. In particular, fixing the average characteristic path length at a higher value would be interesting as the result we have obtained may only hold for smaller values.

Finding an explanation for the non-monotonic dependence of the average synchronization time on the rewiring probability also requires some further work. Using the linearized map of the dynamics may help to discover what is happening. We only used them here to make a comparison with our numerical results. The initial transient behaviour we observed in the decay of the distance $\|\mathbf{d}(t)\|$ from the globally synchronized state (see Figure 9) could also be investigated using the eigenvalues and eigenvectors of the linearized map.

Using a completely different model for the dynamics is another important extension as we have only studied pulse-coupled dynamics. It is possible that the result holds for phase-coupling also. If this is true then our result could be applicable to many real-world dynamical networks and could help in understanding how the topology of these networks relates to the observed synchronization on them.

7 Acknowledgments

The author would like to thank Stefan Grosskinsky for his dedicated supervision of this work and Marc Timme for the initial formulation of the problem and useful discussions. This work has been funded by the EPSRC through the Warwick Complexity Science Doctoral Training Centre.

References

- [1] S.H. Strogatz, Exploring complex networks, *Nature* **410**, 268 (2001)
- [2] M.E.J. Newman, The structure and function of complex networks, *SIAM Rev.* **45**, 2167 (2003)
- [3] R. Albert and A.-L. Barabási, Statistical mechanics of complex networks, *Rev. Mod. Phys.* **74**, 47 (2002)
- [4] S.N. Dorogovtsev and J.F.F. Mendes, Evolution of networks, *Adv. Phys.* **51**, 1079 (2002)
- [5] D.J. Watts and S.H. Strogatz, Collective dynamics of ‘small-world’ networks, *Nature* **393**, 440 (1998)
- [6] M. Barahona and L.M. Pecora, Synchronization in small-world systems, *Phys. Rev. Lett.* **89**, 054101 (2002)
- [7] A. Pikovsky, M. Rosenblum, and J. Kurths, *Synchronization: A universal concept in nonlinear sciences* (Cambridge University Press, Cambridge, UK, 2003)
- [8] S.H. Strogatz, *Sync: The emerging science of spontaneous order* (Penguin Books, London, UK, 2004)
- [9] K. Wiesenfeld, P. Colet, and S.H. Strogatz, Synchronization transitions in a disordered Josephson series array, *Phys. Rev. Lett.* **76**, 404 (1996)
- [10] H.M. Smith, Synchronous flashing of fireflies, *Science* **82**, 151 (1935)
- [11] W. Singer, Neuronal Synchrony: A versatile code review for the definition of relations?, *Neuron* **24**, 49 (1999)
- [12] F. Rieke, D. Warland, R. de Ruyter van Steveninck, and W. Bialek *Spikes: Exploring the neural code* (MIT Press, Cambridge, MA, 1998)
- [13] R.E. Mirollo and S.H. Strogatz, Synchronization of pulse-coupled biological oscillators, *SIAM J. Appl. Math.* **50**, 1645 (1990)
- [14] W. Wu and T. Chen, Desynchronization of pulse-coupled oscillators with delayed excitatory coupling, *Nonlinearity* **20**, 789 (2007)
- [15] G.X. Qi, H.B. Huang, H.J. Wang, X. Zhang, and L. Chen, General conditions for synchronization of pulse-coupled bursting neurons in complex networks, *Europhys. Lett.* **74**, 733 (2006)
- [16] W. Senn and R. Urbanczik, Similar nonleaky integrate-and-fire neurons with instantaneous couplings always synchronize, *SIAM J. Appl. Math.* **61**, 1143 (2000)
- [17] T. Pereira, M.S. Baptista, and J. Kurths, Detecting phase synchronization by localised maps: Application to neural networks, *EPL* **77**, 40006 (2007)
- [18] J.F. Heagy, T.L. Carroll, and L.M. Pecora, Synchronous chaos in coupled oscillator systems, *Phys. Rev. E* **50**, 1874 (1994)
- [19] P.M. Gade and C.-K. Hu, Synchronous chaos in coupled map lattices with small-world interactions, *Phys. Rev. E* **62**, 6409 (1996)
- [20] M. Timme, T. Geisel, and F. Wolf, Speed of synchronization in complex networks of neural oscillators: Analytic results based on random matrix theory, *Chaos* **16**, 015108 (2006)
- [21] H. Hong, B.J. Kim, M.Y. Choi, and H. Park, Factors that predict better synchronizability on complex networks, *Phys. Rev. E* **69**, 067105 (2004)
- [22] J. Vreeken, Spiking neural networks, an introduction, Technical Report UU-CS-2003-008, Institute for Information and Computing Sciences, Utrecht University, (2002). (http://ai-lab.cs.uu.nl/pubs/SNN_Vreeken_Introduction.pdf).
- [23] D.J. Watts, *Small worlds: The dynamics of networks between order and randomness* (Princeton University Press, Princeton, NJ, 1999)
- [24] T. Nishikawa, A.E. Motter, Y.-C. Lai, and F.C. Hoppensteadt, Heterogeneity in oscillator networks: Are small worlds easier to synchronize?, *Phys. Rev. Lett.* **91**, 014101 (2003)
- [25] M. Timme and F. Wolf, The simplest problem in the collective dynamics of neural networks: Is synchrony stable?, *Nonlinearity* **21**, 1579 (2008)
- [26] G. Fagiolo, Clustering in complex directed networks, *Phys. Rev. E* **76**, 026107 (2007)
- [27] J.L. Gross and J. Yellen *Handbook of graph theory* (CRC Press, Florida, 2004)
- [28] M. Denker, M. Timme, M. Diesmann, F. Wolf, and T. Geisel, Breaking synchrony by heterogeneity in complex networks, *Phys. Rev. Lett.* **92**, 074103 (2004)
- [29] M. Barthélemy and L.A.N. Amaral, Small-world networks: Evidence for a crossover picture, *Phys. Rev. Lett.* **82**, 3180 (1999)
- [30] M. Timme, F. Wolf, and T. Geisel, Topological speed limits to network synchronization, *Phys. Rev. Lett.* **92**, 074101 (2004)
- [31] R.A. Horn and C.R. Johnson *Matrix analysis* (Cambridge University Press, Cambridge, UK, 1999)